Analytical Methods

ROYAL SOCIETY OF CHEMISTRY

PAPER

View Article Online
View Journal

Cite this: DOI: 10.1039/d1ay00428j

Anodic near-infrared electrochemiluminescence from Cu-doped CdTe quantum dots for tetracycline detection†

Zhen-Zhen Li,[a] Mei-Xia Wu[b] and Shou-Nian Ding *[a]

Received 14th March 2021
Accepted 13th April 2021

DOI: 10.1039/d1ay00428j

rsc.li/methods

A sensitive anodic near-infrared electrochemiluminescence (ECL) immunosensor for the detection of tetracycline, based on Cu-doped CdTe quantum dots, was fabricated for the first time in this work. We have synthesized Cu-doped CdTe quantum dots by co-precipitation. The emission spectrum of the Cu-doped CdTe quantum dots could reach the near-infrared region at 730 nm in a short reflux time. More importantly, the ECL intensity of the CdTe quantum dots was enhanced by 2 fold after Cu element doping, which was attributed to the Cu d-orbital mixed with the conduction band and valence band of the host CdTe quantum dots. Inspired by the strong anodic ECL intensity of Cu-doped CdTe quantum dots, the anodic near infrared ECL sensor was constructed to detect tetracycline by competitive immunoassay. The detection range of the developed biosensor was 0.01–10 ng mL^{-1} and the detection limit was 0.0030 ng mL^{-1}. In addition, the biosensor showed outstanding selectivity, long-term stability and high reproducibility, which has great potential in the field of analysis and detection.

1. Introduction

Electrochemiluminescence (ECL) has been paid considerable attention due to its high sensitivity, simple instrumentation, low cost, and wide linear range, and has been widely applied in clinical detection, environmental monitoring and food safety.[1] Since Bard[2] firstly reported ECL of silica nanocrystals in 2002, research concerning ECL from nanocrystals has provoked increasing intensive interest. Typically, ECL luminophores concerning quantum dots (QDs), with excellent merits, such as tunable emissions, large stokes shifts, high photochemical stability and prominent biocompatibilities, have drawn considerable attention over the past few decades. However, the basic research of QDs is still mainly concentrated on the visible light region. Due to the excellent penetration of near-infrared light radiation into biological tissues, the potential application value of near-infrared QDs in the field of life science analysis has attracted close attention from the academic community.[3,4] Near-infrared QDs with emission wavelength 650–900 nm have the advantages of both near-infrared windows and QDs. Near-infrared electrochemiluminescence (NECL) can not only provide an alternative to near-infrared fluorescence for the development of low interference biosensors, but also offers a more controllable method for traditional ECL biological detection. Thus, the synthesis of near-infrared QDs with high biological affinity in aqueous systems has important application value and academic significance.[5,6]

As CdTe QDs are an important narrow band gap semiconductor material, there are lots of research studies concentrated on their photoluminescence in the visible light region; however, CdTe QDs with excellent near-infrared properties are still extremely rare. The luminescence properties of CdTe QDs could be improved by forming core–shell QDs,[7] such as CdTe/ZnS QDs, CdTe/CdS QDs or doping with a small amount of other elements,[8,9] such as, Mn, Cu, Zn, and Ni, which provides new ideas for the synthesis of near-infrared luminescent QDs. Importantly, compared with core–shell QDs, the synthesis method of doped QDs is simpler, and doped QDs have attracted considerable attention for wide application potential in terms of their unique optical, electronic, and magnetic properties.[10,11]

Doped QDs not only maintain nearly all advantages of host QDs, but also bring about some new properties, such as larger stokes shifts, wider spectral windows and improved chemical and thermal stability.[12] When dopants are coupled with the host QD crystal field, they are prone to doping energy levels, which makes QDs to exhibit special properties.[13,14] For Mn-doped QDs, their fixed $6A^1$ and $4T^1$ state d–d transition is the main reason to change the properties of QDs.[15] Different from Mn-doped QDs, the emission of Cu-doped QDs mainly comes from the exciton relaxation of the host QDs,[16] which is caused by the recombination between the conduction band of the host QDs and the Cu-induced

[a]Jiangsu Province Hi-Tech Key Laboratory for Bio-medical Research, School of Chemistry and Chemical Engineering, Southeast University, Nanjing 211189, China. E-mail: snding@seu.edu.cn; Fax: +86 25 52090621

[b]Lianshui People's Hospital, Jiangsu 223400, China

† Electronic supplementary information (ESI) available. See DOI: 10.1039/d1ay00428j

impurity state as a result of expanding the emission spectrum range of the QDs.[17] The Cu-doped InP QD emission wavelength covered the entire visible region to the near-infrared region.[18] The maximum emission wavelength of Cu-doped CdS QDs moved to the near-infrared region in aqueous solution.[19] Cu-doped CdTe (Cu:CdTe) QDs have been reported, mainly to study their fluorescence properties.[20] When the Cu element is doped into CdTe QDs, the Cu d state emerged in the valence band and conduction band of the host CdTe QDs, and the holes are transferred to the Cu d-orbital. It changes the original electron–hole recombination path and improved the optical properties of CdTe QDs. However, to our knowledge, Cu:CdTe QD ECL has not been researched so far. Inspired by this, we studied the ECL properties of Cu:CdTe QDs. Cu:CdTe QDs were synthesized in the aqueous phase. Compared with CdTe QDs, the fluorescence wavelength of Cu:CdTe QDs had an obvious red shift. After Cu doping, the anodic ECL of CdTe QDs was enhanced by 2 fold and ECL emission spectra reached near-infrared, at 730 nm. We used Cu:CdTe QDs as an anodic ECL marker for the first time, which has a splendid application prospect in the field of biological immune analysis.

Tetracycline antibiotics as a class of broad-spectrum antibiotics, more than 20 kinds, have been widely applied to human and animal anti-infection treatment. In addition, there is the issue of overuse of antibiotics, which causes residual problems with tetracycline antibiotics around the world. Therefore, the detection and management of tetracycline antibiotics is of vital importance.[21] So far, there have been many methods for the detection of tetracycline antibiotics, such as high performance liquid chromatography[22] (HPLC), high performance liquid chromatography-tandem mass spectrometry[23] (HPLC-MS), capillary electrophoresis[24] (CE), surface enhanced Raman spectroscopy,[25] surface plasma-resonance sensor,[26] and thin layer chromatography[27] (TLC), these detection methods all require professional instruments and relatively complex sample pretreatment. Compared with these methods, the ECL technology is extensively applied in the bioassay field because of its advantages such as simple operation, low background signals and fast response times.[28]

In this work, a NECL immunosensor was constructed to detect tetracycline, which combines the advantages of low near-infrared background signals and sensitive ECL detection. We synthesized Cu:CdTe QDs for use as labeled signals, which had a strong anode NECL signal, and the position of their fluorescence spectrum was consistent with that of the ECL spectrum both at 730 nm, indicating that the surface of the QDs was passivated and there were few surface defects.[29] Due to tetracycline being a small molecule substance, the competition immunoassay was applied to detect tetracycline, and the tetracycline and tetracycline antigen competed with the binding site of the tetracycline antibody, thus establishing the relationship which showed that the ECL intensity of the sensor decreased with the increase of tetracycline concentration in this experiment. Moreover, the obtained results confirmed that the sensor had excellent sensitivity and selectivity. The use of this sensor is expected to be a significant detection method for the analysis and determination of tetracycline.

2. Experimental section

2.1 Reagents and chemicals

Reagents and chemicals are shown in the ESI.†

2.2 Apparatus and measurements

All electrochemical experiments of ECL were carried out on a MPI-M analyzer (Xi'an Ruimai Analytical Instruments Co, Ltd, Xi'an, China). The conventional three-electrode system consists of a modified glassy carbon electrode (GCE, 3 mm in diameter) as the working electrode, a platinum wire as the counter electrode, and a saturated calomel electrode (SCE) as the reference electrode. The ECL spectrum was obtained by using several bandpass filters from 650–800 nm between the PMT and the modified GCE. Other instruments are given in the ESI.†

2.3 Synthesis of water-soluble Cu:CdTe QDs

The MPA-capped Cu:CdTe QDs were synthesized in an aqueous medium according to previous literature.[30] Firstly, 91.3 mg $CdCl_2 \cdot 2.5H_2O$, 21 mg $CuCl_2 \cdot 2H_2O$ and 67.0 μL MPA were mixed in 40 mL of deionized water. The pH of solution was adjusted to 11 with 1 M NaOH under stirring. Meanwhile, fresh NaHTe solution was prepared by the reaction of $NaBH_4$ solution with Te power under a N_2 atmosphere, then 1.0 mL of 0.04 M NaHTe solution was injected into Cd precursor solution. Finally, the reaction mixture was refluxed at 100 °C for 7 h. The obtained Cu:CdTe QD product was precipitated three times using ethanol with centrifugation at 10 000 rpm for 10 minutes. The final precipitates were redissolved in deionized water and then kept in the dark at 4 °C. The CdTe QDs were also obtained using the same method without $CuCl_2 \cdot 2H_2O$.

2.4 Preparation of the Cu:CdTe QDs-Ab probe

QDs-Ab conjugates were prepared according to our previous work.[31,32] Firstly, 75 μL of fresh prepared EDC solution (4.2 mg mL^{-1}) was added to 500 μL Cu:CdTe QDs solution (5 mg mL^{-1}) to activate the carboxyl groups on the surface of QDs. Then, 1 mL of Ab (10 μg mL^{-1}) was added to the above solution, and the solution was gently shaken in the dark at the vortex apparatus at room temperature for 2 h. To remove the uncoupled QDs and by-products, the products were centrifuged (3000 rpm for 10 minutes) with a 50 kD ultrafiltration tube. It should be noted that too much QDs or EDC concentrations will generate aggregates. The final product is stored at 4 °C in the dark for future use.

2.5 Fabrication of the immunosensor

The construction process of the immune sensor is shown in Scheme 1B. Firstly, gold nanoparticles were electrodeposited on a glassy carbon electrode by the potentiometric method, and tetracycline antigen was connected by the Au–S/Au–N bond on the GCE. Then, BSA was modified to seal off the nonspecific

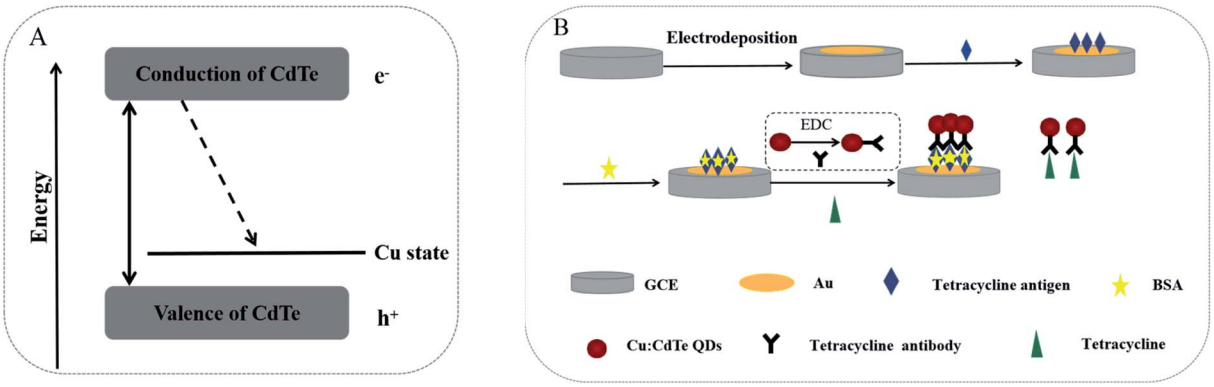

Scheme 1 (A) Luminescence mechanism diagram of Cu:CdTe QDs and (B) preparation process of the ECL sensor.

binding sites on the electrode. Tetracycline and QDs-Ab were simultaneously modified on the electrode, and the tetracycline antigen and the tetracycline compete with the binding site of the tetracycline antibody. The residues on the electrode will be washed away by PBS. Finally, the conjugates of tetracycline antibody and tetracycline antigen were left on the electrode and the ECL intensity of the immunosensor was measured at the electrochemical workstation.

2.6 Preparation of real samples

10 mL pool water was obtained from the pond on the Jiulong Lake Campus and filtered through a filtration membrane (pore size = 0.22 μm). The filtrate was then collected and a series of standard concentrations of tetracycline were added. Milk and honey were bought from the school supermarket. Samples were processed prior to accurate analysis. Milk was treated with trichloroacetic acid to remove proteins and lipids.[33] 300 g L^{-1} trichloroacetic acid was added at 1% (v/v) in milk, sonicated for 20 min, and centrifuged to remove proteins and lipids and the milk was diluted by 20 times with PBS. Honey was needed to be diluted 25 times with PBS. The two actual samples were then filtered using a 0.22 μm membrane, respectively. Finally, a series of test samples with different tetracycline concentrations were prepared by the standard additive recovery method. The corresponding tetracycline concentration was obtained in the actual sample according to the standard curve.

3. Results and discussions

3.1 Characterization of the as-prepared QDs

Fig. 1 exhibits the morphologies of the CdTe QDs and Cu:CdTe QDs. Transmission electron microscope (TEM) images (Fig. 1A and B) demonstrated that both samples presented a good spherical shape. The particle size distribution histogram analyzed the size of the QDs, and it can be seen that the size of the QDs was well uniform, with the average particle size about 4 nm and Cu doping did not change the particle size of the CdTe QDs. The crystal lattice fringes of the QDs can be clearly seen from HRTEM images. The lattice spacing was measured to be 0.36 nm approximately, which corresponds to the (111) plane in the zinc blende structure CdTe QDs.[34] In addition, HRTEM images illustrated that the crystal structure and lattice of CdTe QDs do not change obviously after Cu doping. In addition, the area mapping (Fig. S1†) of QDs was conducted to analyze the element distribution. It can be clearly seen from the mapping that the Cd (green), Te (purple) and Cu (yellow) elements in the QDs were uniformly distributed. The Cu elements were only monitored in the Cu:CdTe QDs, indicating that Cu elements have been successfully doped into CdTe QDs.

The X-ray powder diffraction analysis of the as-prepared CdTe QDs (a) and Cu:CdTe QDs (b) is presented in Fig. S2.† It can be seen from Fig. S2† that the 3 diffraction peaks at 2θ values were 23.9°, 40.2°, and 46.5°, which result from the (111),

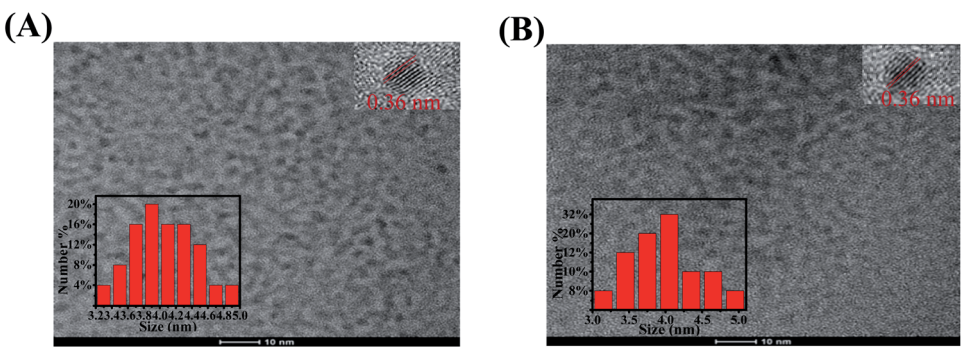

Fig. 1 TEM images of the CdTe QDs (A) and Cu:CdTe QDs (B). Inset shows the HRTEM images and the particle size distribution histogram of the CdTe QDs and Cu:CdTe QDs.

(220) and (311) reflections respectively of inverse spinel structured magnetite. The results were almost consistent with the XRD diffraction peaks at 2θ values of CdTe QDs in reported literature[35] and revealed that QDs exhibited a zinc blende crystal structure. The XRD patterns also indicated that the cubic structure (zinc blende) was well maintained in the CdTe QDs after doping with the Cu element. It illustrated that the incorporation of the impurities could not have changed the lattice structure of the d-dots compared with the host.

Fig. 2A shows the UV-vis spectra of the CdTe and Cu:CdTe QDs. As seen from Fig. 2A, the absorption peak of the CdTe QDs was located at 540 nm, whose emission peak was narrow and symmetrical. The position of the absorption peak of the Cu:CdTe QDs was red-shifted to 650 nm and its peak shape became wider. The results were attributed to Cu element entry into the CdTe QDs lattice and little Cu element replacing the original position of the Cd element. The Cu d level was introduced between the valence band and conduction band of intrinsic CdTe QDs, which changed the original band gap value.[36] The fluorescence emission spectra of the CdTe and Cu:CdTe QDs are illustrated in Fig. 2B. The maximum emission peak positions of the CdTe and Cu:CdTe QDs were respectively located at 670 nm and 730 nm with 360 nm and 450 nm excitation wavelengths correspondingly. Obviously, the position of the fluorescence emission peak of the CdTe QDs was red-shifted after Cu doping and reached the near-infrared region, which is probably attributed to the introduction of the Cu element changing the surface states of the CdTe QDs. The luminescence mechanism diagram[37] of the Cu:CdTe QDs is shown in Scheme 1A. The Cu doping energy level was above the valence band in the CdTe QD band gap, when the QDs absorb the energy of the photons, the electrons transfer from the valence band to the conduction band, and the holes transfer to such a higher Cu doping level, and then the electrons in the conduction band of the host QDs recombine with holes in the Cu-doped energy level. The results would shorten the recombination path of the original electron–hole and cause the red shift of the fluorescence peak position.

The ECL behaviors of the CdTe QDs and Cu:CdTe QDs modified on the glassy carbon electrode (GCE) are shown in Fig. 3A, which were investigated in 0.1 M PBS (pH 7.4) while the potential was scanned from 0 V to +1.50 V at a scan rate of 100 mV s^{-1}. After Cu doping, the ECL intensity of CdTe QDs was increased by 2 fold and the onset potential of the ECL shifted negatively. The enhancement could result from the Cu element doping. The Cu d-orbital mixed with the valence band and conduction band of the host CdTe QDs,[38] and there were more overlaps between the hole and the electron of the CdTe QDs with the localized Cu d levels. It enhanced transfer between the dopant and host levels, which finally enhanced the ECL intensity of the Cu:CdTe QDs.[39] The Cu d levels play the key role in tuning the band gap between the valence band and conduction band of CdTe QDs, resulting in a shortened band gap[40] and enhanced the quantum efficiency of the QD excited states associated with the band gap.[41]

Fig. 3B shows the influence of the Cu doping concentration (n_{Cu}/n_{Cd}) on the ECL intensity. The response of ECL became enhanced with the increase of the Cu doping concentration, from 1.0% to 5.0%, and reached the maximum ECL intensity when the n_{Cu}/n_{Cd} doping percentage was 3.0%, since Cu:CdTe QDs had the most uniform Cu distribution at this doping concentration. When the Cu doping amount was little, with the increase of the Cu doping amount, more Cu entered the CdTe QDs to generate the doping energy level which was located between the valence band and conduction band, as a result of shortening the original electron hole recombination path and enhancing the band gap ECL efficiency. However, when more Cu was added into the CdTe QDs, the ECL intensity decreases reversely. It demonstrated that there were more nonradiative transitions between Cu–Cu. When Cd/Cd = 3.0%, the ECL intensity reached the maximum and the onset potential was the lowest. Therefore, n_{Cu}/n_{Cd} = 3.0% was the best doping concentration in subsequent experiments.

It can be seen from Fig. 3C that when n_{Cu}/n_{Cd} was 3.0%, the positions of the ECL spectrum of the Cu:CdTe QDs recorded by monitoring the ECL intensity of different bandpass filters at 650–800 nm respectively (bandwidth 25 nm) were in the near-infrared region at 730 nm, which was consistent with the PL emission spectra. The results demonstrated that the surface of the prepared Cu:CdTe QDs was well passivated and there were few surface traps. The ECL mechanism of Cu:CdTe QDs mainly was related to the band gap luminescence and confirmed the result of the enhancement ECL intensity of Cu:CdTe QDs.

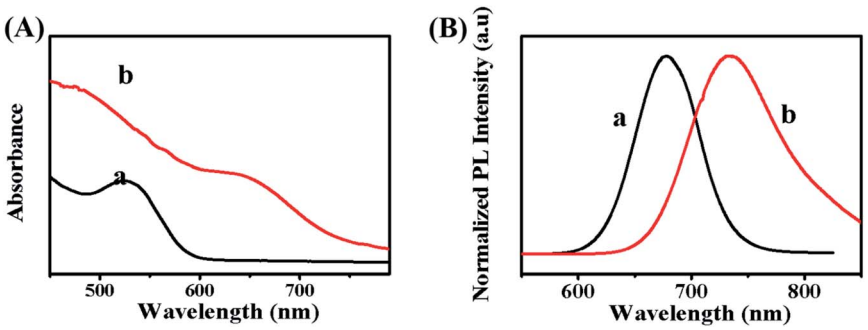

Fig. 2 (A) UV-vis absorption spectra of the CdTe QDs (a) and Cu:CdTe QDs; (b). (B) Fluorescence spectra of the CdTe QDs and Cu:CdTe QDs with 360 nm and 450 nm excitation wavelength correspondingly.

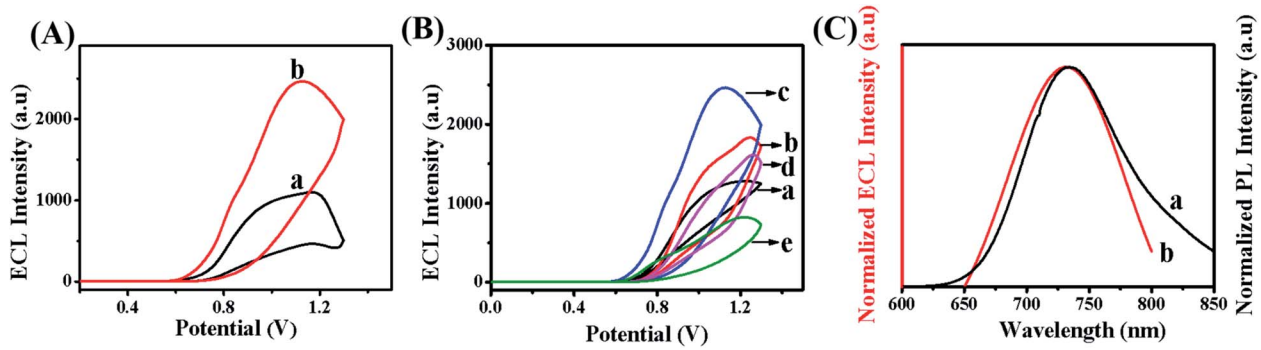

Fig. 3 (A) ECL behavior of the CdTe QDs (a) and Cu:CdTe QDs (b). (B) ECL responses obtained with different doping concentration (a–e): 1.0%, 1.5%, 3.0%, 4.0%, and 5.0%. Cu doping detected in 0.1 M PBS (pH 7.4) containing 20 mM TprA, PMT = 400 V. (C) The PL (a) and ECL spectra (b) of the Cu:CdTe QDs.

3.2 The possible ECL mechanism of Cu:CdTe QDs

In our experiment, with TPrA as the ECL co-reactant, the probable succinct ECL mechanism is similar to the that of a traditional $[Ru(bpy)_3]^{2+}$–TPrA ECL system. TPrA could effectively boost the ECL response of QDs compared with other amines, because of relatively high stability of produced $TPrA^{\bullet}$. The ECL mechanism of Cu:CdTe QDs was the same as that of CdTe QDs. A possible ECL mechanism of Cu:CdTe QDs can be described as follows.[42] Firstly, Cu:CdTe lost an electron through the electrode and formed $Cu:CdTe^{+}$. Meanwhile, TPrA was oxidized to $TPrA^{+\bullet}$, since the radical cation $TPrA^{+\bullet}$ was unstable, the transient state radical cation $TPrA^{+\bullet}$ was considered to lose protons from the carbon, forming a strongly reduced intermediate $TPrA^{\bullet}$. Then, $Cu:CdTe^{+}$ was combined with $TPrA^{\bullet}$ to generate the excited state Cu:CdTe*. Finally, the ECL signal appeared when Cu:CdTe* tuned to Cu:CdTe. The luminescence process of the Cu:CdTe QDs was explained as follows:

$$Cu:CdTe - e^{-} \rightarrow Cu:CdTe^{+} \quad (1)$$

$$TPrA - e^{-} \rightarrow TPrA^{+\bullet} \rightarrow TPrA^{\bullet} + H^{+} \quad (2)$$

$$Cu:CdTe^{+} + TPrA^{\bullet} \rightarrow Cu:CdTe^{*} + TPrA \quad (3)$$

$$Cu:CdTe^{*} \rightarrow Cu:CdTe + h\nu \quad (4)$$

3.3 ECL sensing application of Cu:CdTe QDs

Electrochemical impedance spectroscopy (EIS) was employed to characterize the fabrication process of the sensor. EIS can respond promptly and sensitively to changes in electrode surfaces, so it is usually applied to validate the layer-by-layer assembly process of sensors. As shown in Fig. 4A, each fabrication process of the proposed immunosensor was illustrated by EIS in 0.1 M KCl containing 5 mM $[Fe(CN)_6]^{2-}/[Fe(CN)_6]^{3-}$ solution. The electron transfer resistance (R_{et}) is represented by the semicircle diameter measured by EIS,[43] which could clearly reflect the electron transfer dynamics of the redox probe at the electrode interface. The EIS of the bare electrode displayed an almost straight line (curve *a*), suggesting that the bare electrode had good conductivity. After electroplating a layer of AuNPs on the GCE, the impedance value significantly reduced, which may result from the enhancement of the electron transfer process by AuNPs (R_{et} = 7.5 kΩ curve *b*). Then an increase of R_{et} was observed for the tetracycline antigen modified electrode, because the tetracycline antigen layer blocked the diffusion of the redox probe to the electrode surface (R_{et} = 10.9 kΩ curve *c*). Similarly, the R_{et} value continued to increase after incubating with QDs-Ab (R_{et} = 12.8 kΩ curve *d*), which was due to the introduction of proteins and the formation of immune complexes that act as a barrier to electron transfer. EIS confirmed that the immunosensor was successfully fabricated.

3.4 Optimization of experimental conditions

In order to achieve sensitive detection of tetracycline, optimization was performed for the tetracycline assay using tetracycline as a competitor analyte. According to the traditional ELISA, adding the tetracycline analyte will not affect the experimental results by competitive immunoassay.[44] All the experiments were performed as three parallel experiments as comparison. The related variables (the concentration of TPrA, pH and the concentration of the buffer solution) that affect the strength of Cu:CdTe QD ECL had been optimized. As displayed in Fig. S3A,† when pH varied from 6 to 8, ECL strength reached its highest value at pH 7.4, which was selected as the optimal pH of the buffer solution in the experiment. We have optimized the concentration of PBS, as shown in Fig. S3B;† the ECL intensity of the sensor increased with the increase of the PBS concentration. After reaching 0.1 M, the ECL intensity decreased when the PBS concentration increased. The different concentrations of the PBS buffer would affect the relative position of the buffer and the change of the buffer capacity (for the same ratio). Too high or too low PBS concentrations may change the pH of the solution under external influences, resulting in changes in ECL intensity. Therefore, the optimal concentration of PBS was 0.1 M. It can be seen from Fig. S3C† that the ECL intensity increased immediately with the increase of the TPrA concentration from 5 mM to 50 mM. When the concentration of TPrA was more than 20 mM, the ECL intensity gradually remained

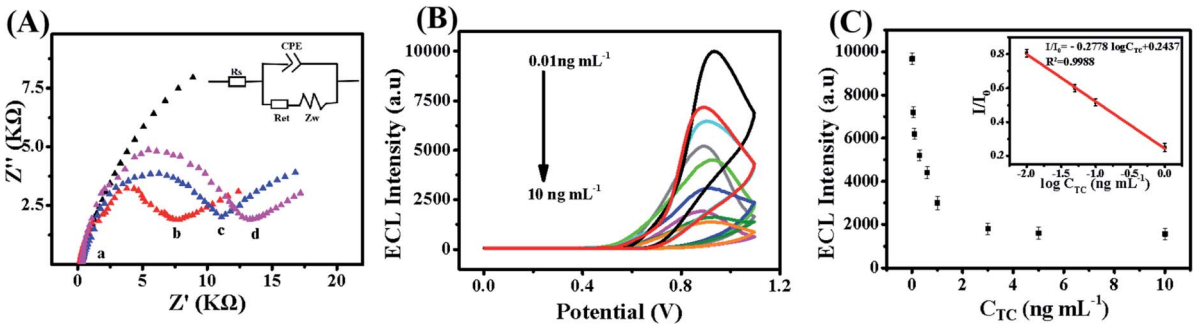

Fig. 4 (A) EIS responses of different modified electrodes: (a) bare GCE (b) GCE/AuNPs (c) GCE/AuNPs/Ag and (d) GCE/AuNPs/Ag/Ab.The inset shows the equivalent circuit applied to fit the impedance data. R_s was the solution resistance; CPE was the constant phase angle element; R_{et} was the electron transfer resistance, and Z_W was the Warburg diffusion resistance. (B) ECL intensity of the sensor in the presence of different concentrations of tetracycline (ng mL^{-1}). (C) Calibration curve of the immune sensor; all the ECL signals were measured in PBS (0.1 M, pH 7.4) containing 20 mM TPrA. The voltage of the PMT was set at 800 V.

stable, and thus 20 mM was the optimal TPrA concentration. The antibody incubation time and temperature would also affect the ECL strength of the immunosensor. Fig. S3D and S3E† show that the ECL intensity became enhanced with the increase of the incubation temperature and incubation time, and reached the maximum at 37 °C and 2 h, respectively, and therefore the optimal incubation time of antibody was 2 h and the optimum incubation temperature was 37 °C for the following experiment.

3.5 Quantitative detection of tetracycline

Under the optimized experimental conditions, we adopted competitive immunoassay to quantitatively detect tetracycline. ECL measurements by PMT were carried out to quantitatively detect tetracycline. All the experiments were performed as three parallel experiments for comparison. ECL intensity decreased with the increase of the tetracycline concentration, and the result is described in Fig. 4B. The ECL intensity of tetracycline is inversely proportional to the logarithmic concentrations of tetracycline presented in Fig. 4C. The linear regression equation was $I/I_0 = -0.2778 \log C_{Tc} + 0.2437$ with the coefficient of determination of 0.9988 (I was the ECL intensity of the sample and I_0 was the ECL intensity of the blank). The linear detection range was 0.01–10 ng mL^{-1}. The detection limit was estimated to be 0.0030 ng mL^{-1} according to the S/N of 3; the detailed calculation process is presented in the ESI.† Table S1† compares the recommended immunosensor with some other assay methods. It can be seen from Table S1† that the detection limit of this method was lowest and had a wider detection range compared to several detection methods. The analysis time of this method was fast and it detected tetracycline in three actual samples, which has wider application potential. In addition, the competitive immunoassay ECL technique had high sensitivity and selectivity. Therefore, our method had certain advantages in the analysis and detection of tetracycline.

3.6 Selectivity, stability and reproducibility of the sensor

We selected cationic Na^+, Ca^{2+}, K^+, anion SO_4^{2-}, NO_3^-, Cl^-, lysine, cysteine, tyrosine, chlortetracycline, oxytetracycline and penicillin as interfering substances to investigate the selectivity of sensors. All the experiments were three parallel experiments for comparison. The interfering substance was prepared with PBS (0.1 M, pH 7.4) solution at a concentration of 100 times that of tetracycline and the concentration of tetracycline was 5 ng mL^{-1}. The reason why we chose the concentration of tetracycline to be 5 ng mL^{-1} was to highlight the competitive relationship between tetracycline antigen and tetracycline, thus forming a clear contrast with the blank sample without tetracycline. Although the ECL intensity of the sensor changed slightly at this concentration, the concentration was still within the linear detection range and conformed to the curve equation formula, so it would not affect the experimental results. Since chlortetracycline, oxytetracycline and tetracycline have similar molecular structures, there was cross-reactivity in the combination with tetracycline antibody. A small amount of chlortetracycline, and oxytetracycline combined with tetracycline antibody, and the combined products were washed away in the subsequent operation, which caused the ECL intensity of the sensor to be reduced. However, the two tetracycline antibiotics had a low cross-reaction rate due to the strong selective specificity of tetracycline antibodies to tetracycline, so they had less interference in the determination of tetracycline and will not significantly affect the specificity of tetracycline antibodies to tetracycline. Other antibiotics such as penicillin will not affect the determination of tetracycline. As can be seen from Fig. 5A, the influence of the above interferents to tetracycline detection was relatively low, indicating that the constructed ECL immunosensor had a good selectivity and was suitable for tetracycline detection.

The stability of the constructed immunosensor shown in Fig. 5B was tested by checking the ECL response periodically. The concentration of tetracycline was 10 pg mL^{-1} in the stability experiments. ECL intensity after being stored for one week at 4 °C retained 96% of the initial value, which illustrated that the immunosensor has accredited stability.

The reproducibility was monitored to confirm its practicality in the sensor system. Firstly, the intra-day reproducibility tests of the sensor were carried out; five sets of sensors were

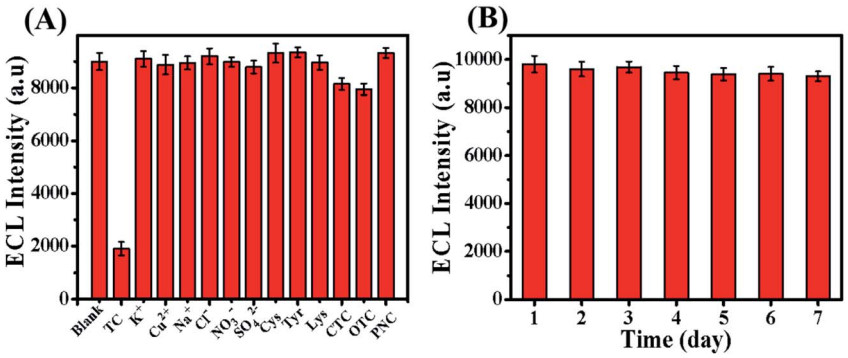

Fig. 5 (A) The selectivity of the constructed sensor under the interference of anionic, cationic, amino acid and other antibiotics. (B) Stability of the immune sensor after preservation for one week.

constructed in parallel with two different concentrations of tetracycline in the same day (80 pg mL^{-1}, 30 pg mL^{-1}), as shown in Fig. S4A and S4B.† It can be seen that the intra-day reproducibility of the sensor was good, with the relative standard deviations (RSD) of 2.83% and 2.75%, respectively. Then, the inter-day reproducibility tests of the sensor are shown in Fig. S4C and S4D.† we constructed five sets of sensors for three consecutive days with different tetracycline concentrations (80 pg mL^{-1}, 30 pg mL^{-1}); it demonstrated that the reproducibility of the sensor in different days was still good, and the relative standard deviations (RSD) were 2.67–2.83% and 2.56–2.75%, respectively. In summary, the immunosensor has good reproducibility.

3.7 Real sample analysis

In order to verify the feasibility of the sensor, we conducted standard addition recovery tests in pond water, honey and milk respectively. All the experiments were three parallel experiments for comparison. The state-specified standard of tetracycline in milk and honey is not more than 100 μg kg^{-1}, 50 μg kg^{-1}. The detection limit of this method is 0.0030 ng mL^{-1}, which is far lower than the minimum residual amount of tetracycline in the sample. Therefore, this method is suitable for the detection of the tetracycline content in the sample. A certain amount of tetracycline was added to the above samples and a series of actual samples with different tetracycline concentration gradients were obtained and are shown in Table S2.† The standard addition method was carried out to test the recovery of the developed immunosensor and the results showed that the recovery was between 95.77% and 105.70%, and the RSD ranged from 1.24% and 5.70% in the three actual samples. The results manifested that the sensor had high accuracy and could be applied to the detection of tetracycline in actual samples. In the actual sample test, we compared the test results of this method with those of the standard ELISA. From Table S2,† it can be seen that the accuracy of the test value, the recovery and the relative standard deviation (RSD) value of this method were very close to those of ELISA. Therefore, it is believed that this method can be applied to the detection of tetracycline in actual samples.

4. Conclusion

In summary, a prospective NECL immunosensor was proposed for tetracycline detection based on Cu:CdTe QDs. Due to the mixing of the Cu d-orbital with the valence band and conduction band of the CdTe QDs, the luminescence properties of the Cu:CdTe QDs originate from exciton relaxation *via* transition from the conduction band of the CdTe QDs to the Cu d-level. Thus the emission spectrum of the Cu:CdTe QDs could reach the near-infrared region at 730 nm and the CdTe QDs ECL intensity increased by 2 fold. The emission wavelength of QDs reaches the near-infrared region, which reduces the interference of background signals and strengthens the penetration of near-infrared light into biological tissues. Therefore, Cu:CdTe QDs will have more extensive applications. The improvement of the ECL strength of CdTe QDS could enhance their sensitivity in analysis and detection. The Cu:CdTe QDs were applied as the NECL signal markers in the sensor to detect tetracycline, and the biosensor had outstanding stability, selectivity and reproducibility. More importantly, compared to other detection methods, the immunosensor in this experiment has a lower detection limit, which could realize sensitive detection of tetracycline and has great research significance. In addition, this method to detect tetracycline is more convenient and faster, and it is expected to become an important detection method in the field of analysis.

Conflicts of interest

The authors declare no competing financial interest.

Acknowledgements

This work was supported by the National Key Research and Development Program of China (2017YFA0700404), the National Science and Technology Major Project (AWS17J016, and 2019SWAQ05-5-4), the National Natural Science Foundation of China (21535003, and 21575022), and the Key Research & Development Plan of Jiangsu Province (BE2018617).

References

1 W. Miao, *Chem. Rev.*, 2008, **108**, 2506–2553.
2 Z.-F. Ding, B. M. Quinn, S.-K. Haram, L.-E. Pell, B. A. Korgel and A. J. Bard, *Science*, 2002, **296**, 1293–1297.
3 J. Wang and H. Han, *J. Colloid Interface Sci.*, 2010, **351**, 83–87.
4 M. Z. Yu, K. L. Zhao, X. H. Zhu, S. Y. Tang, Z. Nie, Y. Huang, P. Zhao and S. Z. Yao, *Biosens. Bioelectron.*, 2017, **95**, 41–47.
5 Y.-F. Liu, W. Chen, A. G. Joly, Y. Q. Wang, C. Pope, Y. B. Zhang, J. O. Bovin and P. Sherwood, *J. Phys. Chem. B*, 2006, **110**, 16992–17000.
6 K. Shao, B. R. Wang, S. Y. Ye, Y. P. Zuo, L. Wu, Q. Li, Z. C. Lu, X. C. Tan and H. Y. Han, *Anal. Chem.*, 2016, **88**, 8179–8187.
7 J. Wang and X. Jiang, *Sens. Actuators, B*, 2015, **207**, 552–555.
8 F. Zhang, F. He, X.-W. He, W.-Y. Li and Y.-K. Zhang, *Luminescence*, 2014, **29**, 1059–1065.
9 S. L. Li, P. Jiang, S. Y. Hua, F. L. Jiang and Y. Liu, *Nanoscale*, 2021, **13**, 3673–3685.
10 P. Singh, R. K. Singh and R. Kumar, *RSC Adv.*, 2021, **11**, 2512–2545.
11 N. T. Hien, N. X. Ca, N. T. Kien, N. T. Luyen, P. V. Do, L. D. Thanh, H. T. Van, S. Bharti, Y. Wang, N. T. M. Thuy and P. M. Tan, *J. Phys. Chem. Solids*, 2020, **147**, 109638.
12 N. Pradhan, S. Das Adhikari, A. Nag and D. D. Sarma, *Angew. Chem.*, 2017, **56**, 7038–7054.
13 R. G. Chaudhuri and S. Paria, *Chem. Rev.*, 2012, **112**, 2373–2433.
14 A. N. Yadav, A. K. Singh, D. Chauhan, P. R. Solanki, P. Kumar and K. Singh, *New J. Chem.*, 2020, **44**, 13529–13533.
15 S. Mabrouk, H. Rinnert, L. Balan, S. Blanchard, J. Jasniewski, G. Medjahdi, R. Ben Chaabane and R. Schneider, *J. Alloys Compd.*, 2021, **858**, 158315.
16 W. Zhang, Q. Lou, W. Ji, J. Zhao and X. Zhong, *Chem. Mater.*, 2014, **26**, 1204–1212.
17 B. B. Srivastava, S. Jana and N. Pradhan, *J. Am. Chem. Soc.*, 2011, **133**, 1007–1015.
18 N. X. Ca, H. T. Van, P. V. Do, L. D. Thanh, P. M. Tan, N. X. Truong, V. T. K. Oanh, N. T. Binh and N. T. Hien, *RSC Adv.*, 2020, **10**, 25618–25628.
19 F. Zhang, X.-W. He, W.-Y. Li and Y.-K. Zhang, *J. Mater. Chem.*, 2012, **22**, 22250–22257.
20 D. Grecu, A. D. Compaan, D. Young, U. Jayamaha and D. H. Rose, *J. Appl. Phys.*, 2000, **88**, 2490–2496.
21 I. Chopra and M. Roberts, *Microbiol. Mol. Biol. Rev.*, 2001, **65**, 232–260.
22 Y. Liu, H.-L. Yang, S. Yang, Q.-W. Hu, H.-B. Cheng, H.-Y. Liu and Y.-S. Qiu, *J. Chromatogr. B: Anal. Technol. Biomed. Life Sci.*, 2013, **917**, 11–17.
23 H.-C. Liu, L.-G. Chen and J. Ding, *Microchim. Acta*, 2017, **184**, 4091–4098.
24 G. Islas, J. A. Rodriguez, I. Perez-Silva, J. M. Miranda and I. S. Ibarra, *J. Anal. Methods Chem.*, 2018, **2018**, 5394527.
25 R. Li, H. Zhang, Q.-W. Chen, N. Yan and H. Wang, *Analyst*, 2011, **136**, 2527–2532.
26 R. Verma and B. D. Gupta, *Analyst*, 2013, **138**, 7254–7263.
27 I. Meisen, S. Wisholzer, J. Soltwisch, K. Dreisewerd, M. Mormann, J. Muthing, H. Karch and A. W. Friedrich, *Anal. Bioanal. Chem.*, 2010, **398**, 2821–2831.
28 Y. Hu, L. Su, S. Wang, Z. Guo, Y. Hu and H. Xie, *Microchim. Acta*, 2019, **186**, 512–521.
29 S. Liu, X. Zhang, Y. Yu and G. Zou, *Biosens. Bioelectron.*, 2014, **55**, 203–208.
30 L. Zou, Z. Gu, N. Zhang, Y. Zhang, Z. Fang, W. Zhu and X. Zhong, *J. Mater. Chem.*, 2008, **18**, 2807–2815.
31 R. Cui, H.-C. Pan, J.-J. Zhu and H.-Y. Chen, *Anal. Chem.*, 2007, **79**, 8494–8501.
32 E. Song, M. Yu, Y. Wang, W. Hu, D. Cheng, M. T. Swihart and Y. Song, *Biosens. Bioelectron.*, 2015, **72**, 320–325.
33 L. Jia, S. Guo, J. Xu, X. Chen, T. Zhu and T. Zhao, *Nanomaterials*, 2019, **9**, 976.
34 N. Gaponik, D. V. Talapin, A. L. Rogach, K. Hoppe, E. V. Shevchenko, A. Kornowski, A. Eychmuller and H. Weller, *J. Phys. Chem. B*, 2002, **106**, 7177–7185.
35 H. Zhang, Z. Zhou, B. Yang and M. Y. Gao, *J. Phys. Chem. B*, 2003, **107**, 8–13.
36 C. Chen, P. Zhang, G. Gao, D. Gao, Y. Yang, H. Liu, Y. Wang, P. Gong and L. Cai, *Adv. Mater.*, 2014, **26**, 6313–6317.
37 G. K. Grandhi, R. Tomar and R. Viswanatha, *ACS Nano*, 2012, **6**, 9751–9763.
38 J. Wang, Y.-Y. Zhang, W.-W. Zhao, J.-J. Xu and H.-Y. Chen, *Electroanalysis*, 2013, **25**, 951–958.
39 S. Sapra, A. Prakash, A. Ghangrekar, N. Periasamy and D. D. Sarma, *J. Phys. Chem. B*, 2005, **109**, 1663–1668.
40 F.-F. Wu, Y. Zhou, J. X. Wang, Y. Zhuo, R. Yuan and Y. Q. Chai, *Sens. Actuators, B*, 2017, **243**, 1067–1074.
41 S.-N. Ding, Y. Jin, X. Chen and N. Bao, *Electrochem. Commun.*, 2015, **55**, 30–33.
42 X.-F. Wang, J.-J. Xu and H.-Y. Chen, *J. Phys. Chem. C*, 2008, **112**, 17581–17585.
43 H. Li, J. Yan, W. Ou, H. Liu, S. Liu and Y. Wan, *Biosens. Bioelectron.*, 2015, **64**, 111–118.
44 N. Pastor-Navarro, S. Morais, A. Maquieira and R. Puchades, *Anal. Chim. Acta*, 2007, **594**, 211–218.

